BaoYu Zong[a], YuPing Wu[a], Nguyen Nguyen Phuoc[a], Pin Ho[b], JinJun Qiu[b], Yi Yang[b], Miao Jun Chua[a], Wei Beng Ng[a], YunJie Chen[b], GuChang Han[b]
[a] Temasek Laboratories, National University of Singapore, Singapore
[b] Data Storage Institute, Agency for Science, Technology and Research (A*STAR), Singapore

Quick fabrication of appropriate morphology and composition CoFe films with desirable microwave properties

A methodology to quickly prepare CoFe nanofilms with large magnetic permeability and resonance frequency from simple salt solutions is demonstrated. As the microwave properties of thin films are largely determined by their surface morphology and composition, CoFe film with unique morphology and composition is proposed based on theoretical analysis and subsequently electrodeposited with suitable parameters. This approach reveals that Fe_xCo_{1-x} ($0.3 < x < 0.5$ in atomic ratio) films consisting of sub-30 nm spherical nanoparticles, even in the form of bigger aggregated-nanoparticles, usually show a low coercivity ($\leq 4\,240$ A · m^{-1}), moderate magnetic anisotropy (2 900–8 580 A · m^{-1}), and high magnetic moment (≥1.4 T), permeability (>200) as well as resonance frequency (>1 GHz). Further experimental analyses show root causes of the phenomena. This methodology also provides useful references to rapidly identify microwave properties of thin films from their surface morphologies and main electrodeposition parameters.

Keywords: Nanofilm electrodepostion; Synthesis design; Permeability and resonance frequency; GHz microwave application; Morphology and composition

1. Introduction

As one type of functional materials, thin soft ferromagnetic films are intensively used in numerous advanced areas, such as in ultrahigh density data storage and ultrathin gigahertz (GHz) frequency devices, due to their achievable compact and light-weight core-elements with excellent performance [1–3]. To cater to rapid development and production of the devices, investigating effective simple methods to prepare thin films with appropriate properties and probing the internal microwave properties from the surface morphology and fabrication parameters of the films are in demand and interesting to researchers and engineers [4, 5]. Thin films prepared from different tools or parameters usually exhibit diverse morphologies, such as smooth or rough surfaces, irregularly or regularly (e.g., spherical) shaped particles contained, etc. [6–8]. The surface morphology of the thin film is representative of its crystallographic structure and composition [9–11]. Since magnetic microwave properties are determined by the particle size, composition, and lattice constant of crystals [12–14], thin films with different morphologies may exhibit different unique magnetic microwave properties. Previous investigations on electrodeposited thin Fe-based films demonstrate that the deposition parameters (e.g., composition, *pH*, and additive of plating solution, plating current) and substrate affected both the surface morphologies and internal physicochemical or magnetic microwave properties [15–18]. As such, through theoretical analysis to determine the appropriate morphology and composition as well as selecting suitable deposition parameters, it is possible to develop a quick and cost-efficient process to fabricate thin soft ferromagnetic films with desirable microwave properties. Previous study results also supply some background on the theoretical analysis of static magnetism and dynamic microwave properties [19–22]. By using this simple practical fabrication route, excess characterization and process time required in conventional development approaches or industrial mass-productions [1, 2] can be avoided. In addition, through analyzing the experimental results from fine tuning the deposition parameters for in-depth understanding of the relationships between the morphology and physicochemical, static magnetism as well as dynamic microwave properties, a convenient method to quickly determine the properties of thin films from their deposition parameters and surface morphologies may also be established.

Herein we demonstrated thin Fe_xCo_{1-x} ($0.3 < x < 0.5$ in atomic ratio) nanoparticle films, quickly synthesized from simple sulfate/chloride-based solutions, possessing desirable static and dynamic magnetic properties, such as large saturation magnetization (M_s, up to 2.2 T), magnetic permeability (μ, real part >200), and resonance frequency (f_r, >1 GHz). As opposed to conventional fabrication methods via the selection of final fabricated products, the rapid preparation of the thin films with desired properties was based on initial suggestion of their ideal morphology and composition from theoretical understandings, as well as subsequent selection of suitable fabrication process and parameters. The effects of plating current density I_d, solution composition, and temperature on the morphology were further investigated as well.

2. Experimental methods

In this investigation, CoFe films were electrodeposited on Si wafers. A seed layer of Ta 5 nm/Au(110) 30 nm was first

deposited on each Si wafer using a sputter system (MPS-6301-SP, ULVAC, Japan). This seed layer acted as an electrical conducting layer for the electrodeposition. The CoFe films were fabricated from a 1.3l Paddle-Cell (Technic, Singapore) with a DC power supply using our previously developed simple salt solution, containing 0.095 M $FeSO_4 \cdot 7H_2O$, 0.10 M $CoSO_4 \cdot 7H_2O$, 0.90 M NH_4Cl, 0.5 M H_3BO_3 at 40 °C or room temperature (*RT*) [23]. An organic additive of dimethylamine borane [$(CH_3)_2NHBH_3$, DMAB, Bayer, Germany] was added to the solution during the electroplating process. During the electrodeposition of the CoFe films (with 100–400 nm in thickness), a range of plating current density (I_d) from 7.5 to 25.0 mA · cm^{-2} was adopted, and a magnetic field of 22 400–24 000 A · m^{-1} was applied parallel to the substrate surface to induce an in-plane uniaxial anisotropy (H_k), which energy effect is usually connected to the existence of only easy direction and allows magnetization direction of any domain along the easy axis of hysteresis loop.

The thickness of the films was measured using a surface profiler (Taylor Hobson, FormTalySurf 50, UK) or an atomic force microscope (AFM, Dimension 3100, USA). The morphologies of the films were examined with a field emission scanning electron microscope (FESEM, JSM 7401F, JEOL, Japan) or AFM. The stoichiometry of the electrodeposited films was determined by means of energy dispersive X-ray spectroscopy (EDX), which was attached to the FESEM. The crystallographic texture of the films was evaluated from X-ray diffraction (XRD, UltimaIV, Rigaku, Japan) using a Philips X'pert diffractometer (λ = 1.5406 Å, Bragg–Brentano geometry, PW3088/60 (line focus) Cu MRD PFX mirror, without filter and monochromator), and recorded at a scanning rate of 0.02° s^{-1} in the 2θ ranging from 30 to 80°. The bulk resistivity ρ of the film, calculated by dividing the sheet resistance with the film thickness, was measured using a four point probe head (RT-70, NAPSON, Japan). A vibrating sample magnetometer (VSM, EV-7, USA) was used to measure the saturation magnetization (M_s) and coercivity (H_c). The M_s was obtained from the non-normalized saturation magnetization (M_0) indicated in the measured *M–H* loop. The permeability frequency spectra from 0.9 to 10 GHz were measured with a vector network analyser (Agilent 5230A, USA). All the calculation methods after the measurements can be found in previous works [15, 23].

3. Results and discussion

Ferromagnetic CoFe nanofilms with desirable microwave properties were fabricated from different simple sulfate/chloride-based solutions with optimized parameters.

3.1. Ideal morphology and composition of thin film from theoretical analyses

Based on theoretical analyses as follows, thin Fe_xCo_{1-x} ($0.3 < x < 0.5$ in atomic ratio) films, consisting of fine spherical nanoparticles, could display desirable microwave properties, such as high complex magnetic permeability (μ) and large linear resonance frequency (f_r). As prepared under an induction of the applied magnetic field, the thin films exhibited a uniaxial in-plane anisotropy. The relationship between their static and dynamic magnetic properties could be explained using Acher's law (1) [24] and the standard Lorentzian equation (Eq. (2)) [25], as shown in the following:

$$(\mu_s - 1)f_r^2 = (\gamma' M_s)^2 \quad (1)$$

$$\mu(\omega) = 1 + (\mu_s - 1)/[1 + i\omega/\omega_a - (\omega/\omega_r)^2] \quad (2)$$

Where the static permeability, $\mu_s = 1 + 4\pi M_0/H_k = 1 + M_s/H_k$, γ' is the gyromagnetic factor (a constant coefficient, ~3 MH$_z$ Oe^{-1} for ferromagnets, such as the CoFe), ω, ω_r, and ω_a represent the circular, resonance, and characteristic relaxation frequencies of the incident wave, respectively. For ferromagnetic materials with high M_s (e. g., CoFe), since $H_k << M_s$, μ_s is expected to be >> 1 (viz., $\mu_s \approx M_s/H_k$). Substituting it into (1) and (2), gives equations as follows:

$$f_r = \gamma'(M_s H_k)^{1/2} \quad (3)$$

$$\mu(\omega) = 1 + M_s/[H_k(1 + i\omega/\omega_a - \omega^2/\omega_r^2)] \quad (4)$$

Therefore, to achieve desirable microwave properties with large μ and f_r, thin film must exhibit a high M_s, low H_c, and moderate H_k.

CoFe has been selected as the material of interest as it displays the highest saturation magnetization or magnetic moment ($M_s \sim 2.45$ T) theoretically and low H_c (down to <1 600 A · m^{-1}) [25, 26]. Previous works show that for a CoFe film with a relatively high Fe content of 30–70 %, the large M_s can be realized [23, 26]. In addition, a film containing higher Co levels demonstrates a larger crystallinity and magnetic anisotropy H_k (>3 200 A · m^{-1}) than lower Co-content materials [27, 28]. Intuitively, the Co content in the CoFe film should ideally be higher than that of Fe (viz. $x < 0.5$ for Fe_xCo_{1-x} film). Previous reports have also shown that thin magnetic soft films consisting of uniform fine spherical nanoparticles typically display a lower coercivity H_c, as there is existing strong exchange-coupling among these fine nanoparticles with homogeneous grain domain structures [23, 29]. As such, to achieve films with desirable static magnetism and dynamic microwave properties, besides optimizing the Fe and Co content in thin Fe_xCo_{1-x} films to be in the range of $0.3 < x < 0.5$ (in atomic ratio), the fabrication process should be geared towards producing uniform fine spherical nanoparticles. High M_s CoFe alloy films with such morphology have been obtained by optimizing DMAB concentration in our previous work using a similar plating solution. However, the effects of other plating parameters and the associated microwave properties were unclear and not investigated [23].

3.2. Preparation of CoFe films with unique morphology

Electrodeposition was also chosen to quickly prepare the unique morphology films due to its short processing time, cost-effectiveness, and flexibility to manufacture large sheets of magnetic films [22, 30, 31]. Figure 1 schematically illustrates the rapid preparation process to achieve the thin CoFe films, consisting of uniform fine nanoparticles, from the simple solution with similar concentration of Fe^{2+} and Co^{2+} with suitable higher I_d. During electrodepositions of Fe-series alloys, as anomalous co-deposition

usually exists [32, 33] and similar concentrations of Fe^{2+} and Co^{2+} can lead to a co-deposited CoFe alloy with similar ratio of Fe and Co [34], a plating solution with similar $[Fe^{2+}]$ and $[Co^{2+}]$ of 0.095 M and 0.10 M, respectively [23], was thus selected for achieving the Fe_xCo_{1-x} films with the desired composition ($0.3 < x < 0.5$). Moreover, from the kinetics viewpoint of crystal growth, intensive initial crystallite nucleation was critical for achieving uniform particle films. Although substrate surface conditions, component type and concentration of the electrolyte, and other factors can affect the crystal growth (e. g., suitable organic additives reducing surface tension of the substrate and leading to easier crystallite nucleation), plating current density is a generally effective means to control the crystal growth for different plating solutions and substrates [7, 35]. Thus, a relatively high I_d (e. g., reaching the middle range of the plating I_d window where shiny silver surfaces are obtained for the films) during electrodeposition was used to achieve the high density of initial crystallite nucleation, and subsequently led to the desirable unique morphology films. Based on these suggested plating parameters, a series of thin CoFe films were subsequently synthesized from the simple sulfate/chloride-based solutions at different temperatures, in the presence and absence of the organic additive. For comparison, different values of I_d were also used.

As shown in Fig. 2, CoFe films with different morphologies were prepared from four simple solutions at various I_d. The different nanomorphologies of the thin films were attributed to the solution component (e. g., additive) and *pH*, solution temperature and plating I_d [17, 23]. Notably, the

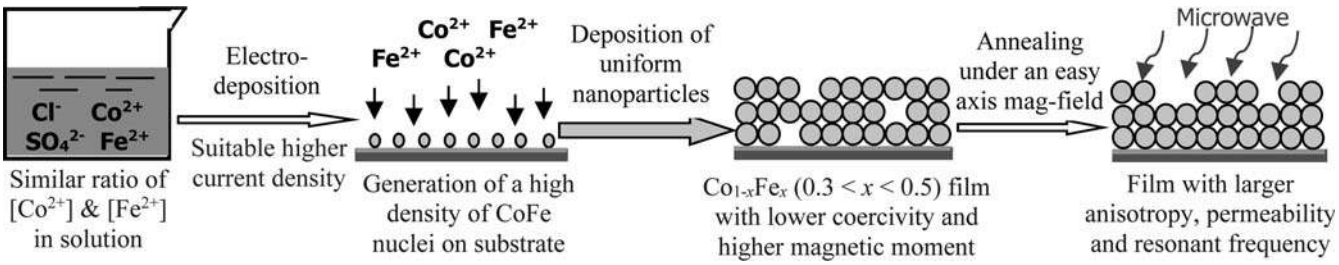

Fig. 1. Schematic illustration of preparation of thin CoFe film with desirable microwave properties through electrodeposition from a simple sulfate and chloride salt solution.

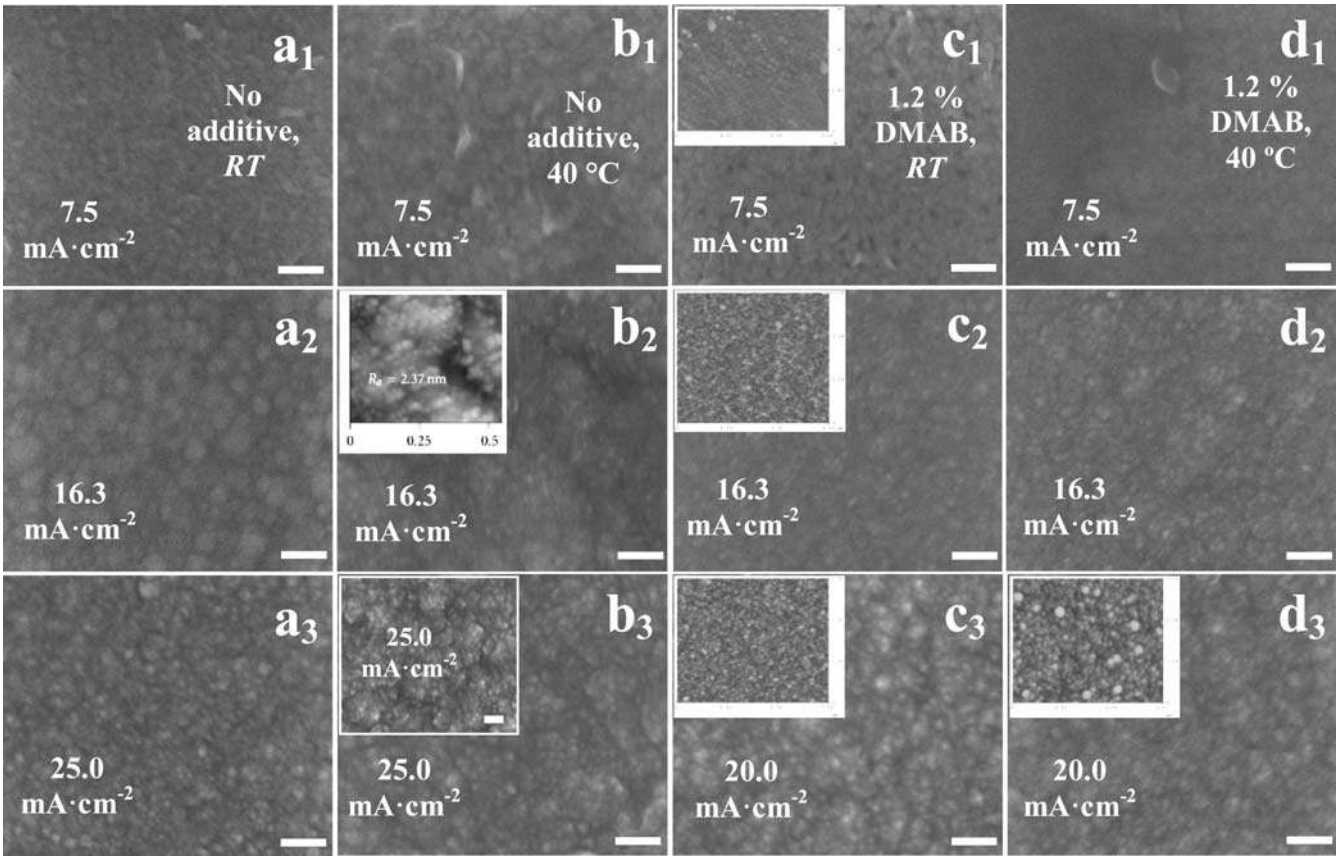

Fig. 2. FESEM images of the four series of thin CoFe films, electrodeposited from the solution: without additive at *RT* (a_1–a_3) or 40 °C (b_1–b_3) and a current density I_d of 7.5, 16.3, and 25.0 mA · cm^{-2}, respectively. The inset image of (b_2) is the corresponding 0.6 × 0.6 μm AFM magnification image; (c_1–c_3) and the inset of (b_3) containing 1.2 % DMAB additive at *RT* and an I_d of 7.5, 16.3, 20.0, and 25.0 mA · cm^{-2}, respectively, while the insets of (c_1–c_3) and (d_3) are the corresponding 3 × 3 μm AFM film images; (d_1–d_3) containing 1.2 % DMAB additive at 40 °C and an I_d of 7.5, 16.3, and 20.0 mA · cm^{-2}, respectively. The scale bars in the FESEM images are 100 nm.

pH value of the solution was largely determined by the H_3BO_3 buffer-acid and DMAB additive, and a value of ~3.0 or 4.0 (due to the hydrolysis of DMAB [36]) for the H_3BO_3-contained solution in the absence and presence of 1.2 % DMAB, respectively, was obtained. When comparing Fig. 2a–d series films, which were deposited at the same I_d from the different solutions – without additive at *RT* (*pH* ~ 3.0) or 40 °C (*pH* ~ 3.0), containing 1.2 % DMAB at *RT* (*pH* ~ 4.0) or 40 °C (*pH* ~ 4.1), respectively, although the addition of DMAB additive and change of solution temperature could slightly vary CoFe particle sizes in the films (e. g., from Fig. $2a_1$–a_3 to d_1–d_3, respectively) via slightly changing Fe^{2+} and Co^{2+} reduction potentials on the cathode electrode [15, 36], the changes in plating I_d exerted the most influence on the CoFe particle size and surface morphology, just as reported in Refs. [7, 35]. In particular, the varying trends of the particle shape and size in the CoFe films with I_d for all four plating solutions were consistent.

The morphologies in Fig. $2a_1$–d_1 show that the CoFe films prepared at lower I_d were made up of non-uniform, irregularly-shaped particles. With the increase in I_d, the nanoparticles in the films (Fig. $2a_2$–d_2) became relatively more uniform in size (about 20 – 30 nm) and increasingly spherical in shape. This change was consistent with the suggestion from the above theoretical analysis. At a lower I_d, fewer initial nuclei were produced on the substrates. This subsequently resulted in non-uniform crystal growth where the different non-uniformly distributed nuclei merged with increasing deposition time. In contrast, a higher I_d generated much more nuclei initially, higher overpotential and reduced ion diffusion thickness on the substrate surface, which contributed to more even current distribution and finer grain particles [33, 35] on the substrates. As a result, this led to a more uniform growth of CoFe crystals or particles. The inset of Fig. $2b_2$, a magnified image obtained using the high resolution of the AFM system, shows some fine nanoparticles aggregating into bigger nanoparticles (>30 nm) as well. When the I_d was further increased, both the aggregated and fine particle sizes grew in size. For example, for the series (c) films, both FESEM and AFM images showed such similar observations. When the I_d was increased from 16.3 to 20.0, and finally to 25.0 mA · cm^{-2}, the aggregated particle size increased from approximately 50 to 90, and finally to 110 nm (depicted in Fig. $2c_2$, c_3, and inset of b_3), respectively, while the size of the elemental fine particles also slightly increased. For the series (a), (b), and (d) films deposited from other three different solutions, similar trends of particle size against I_d are also illustrated in Fig. $2a_1$–a_3, b_1–b_3, and d_1–d_3, respectively. Therefore, despite the different morphologies and particle sizes prepared from different solutions due to the diverse effects of additive and solution temperature, a thin CoFe nanofilm comprising relatively uniform fine spherical nanoparticles could be readily and repeatedly prepared from the different simple sulfate/chloride-based solutions by tuning the plating current density I_d.

3.3. Morphology implication and experimental clarification of magnetic microwave properties

Since CoFe films with desirable unique morphology have been rapidly electrodeposited by using the selected suitable ratio of $[Fe^{2+}]$:$[Co^{2+}]$ and relatively high I_d, these thin CoFe nanofilms were further examined to test if they possessed appropriate magnetic microwave properties. Comparison analyses for all the CoFe films, including those consisting of the irregular shape particles, from the four plating solutions were also carried out to understand the relationship between the film morphology and microwave properties. The results are given in Table 1. In accordance with the above theoretical analyses, the thin magnetic films consisting of uniform fine spherical nanoparticles, such as in Fig. $2a_2$–d_2, would display lower coercivity, H_c. The CoFe films with slightly larger spherical nanoparticles (e. g., in Fig. $2a_3$–d_3) were also expected to have lower H_c compared to those films with irregularly-shaped particles in Fig. $2a_1$–d_1. The characterization results showed that a low H_c of down to 640 A · m^{-1} was obtained for the films in Fig. $2a_2$–d_2, while the H_c (880 – 10320 A · m^{-1}) for the films in Fig. $2a_3$–d_3 was lower than the H_c (1840 – 10560 A · m^{-1}) of the films in Fig. $2a_1$–d_1. Moreover, as the $[Fe^{2+}]$ and $[Co^{2+}]$ concentrations were similar in each

Table 1. Static magnetism and dynamic microwave (shaded part) properties of CoFe films prepared using different current densities in four different solutions.

Plating solution	I_d (mA · cm^{-2})	Co : Fe (atom)	$H_{c\text{-}easy}$ (A · m^{-1})	$H_{c\text{-}hard}$ (A · m^{-1})	M_s (T)	H_k (A · m^{-1})	μ'_{max}	μ''_{max}	f_r (GHz)	f_{rEsti} (GHz)
a) Without additive, *RT*, *pH*3.0	7.5	68 : 32	4400	4240	0.6	4640	72	40	1.1	1.7
	16.3	62 : 38	1120	900	1.6	3000	455	323	1.9	2.3
	25.0	60 : 40	1760	1680	1.4	290	356	171	1.6	2.1
b) Without additive, 40 °C, *pH*3.0	7.5	70 : 30	10560	10560	0.3	0	24	N.A.	N.A.	N.A.
	16.3	63 : 37	4240	2000	1.5	6240	318	241	3.1	3.3
	25.0	59 : 41	10320	10320	0.7	0	61	58	N.A.	N.A.
c) 1.2 % DMAB, *RT*, *pH*4.0	7.5	67 : 33	4400	4000	1.4	6600	101	62	2.6	3.2
	16.3	57 : 43	880	640	2.2	7360	441	355	3.9	4.3
	20.0	56 : 44	1600	1760	1.8	6000	303	210	3.1	3.5
	25.0	55 : 45	1680	1360	.6	4800	225	162	2.3	2.9
d) 1.2 % DMAB, 40 °C, *pH*4.1	7.5	62 : 38	2640	1840	1.6	6160	159	125	2.6	3.3
	16.3	58 : 42	1600	880	2.2	8580	250	186	4.5	4.6
	20.0	56 : 44	880	1040	1.9	6400	121	79	3.3	3.7

plating solution, the anomalously co-deposited films from the solutions should possess a relatively high atomic ratio of Fe (e. g., >25 %), particularly for the films prepared from a middle and higher range of I_d [2, 33] (e. g., in Fig. $2a_2$–d_2 and a_3–d_3). As such, these CoFe films should display high M_s if the Fe and Co atoms were closely and uniformly distributed across the entire alloy films.

The experimental data in Table 1 demonstrate that all the films from the four plating solutions contained a relatively high Fe atom-ratio (30 – 48 %). The thin CoFe films, which were made up of fine or aggregated particles and fabricated using a relatively high I_d (shown in Fig. $2a_2$–d_2, a_3, c_3, inset of b_3, and d_3), exhibited high M_s of 1.5 – 2.2 T. Despite existing anomalous co-deposition for the Fe^{2+} and Co^{2+} reductions, the individual standard electrode potential of the metal-ion couple, representing the driving force extent in reduction, is still the main factor to determine the reduced Fe : Co ratio in the CoFe alloy [7, 11]. Since Fe^{2+} and Co^{2+}

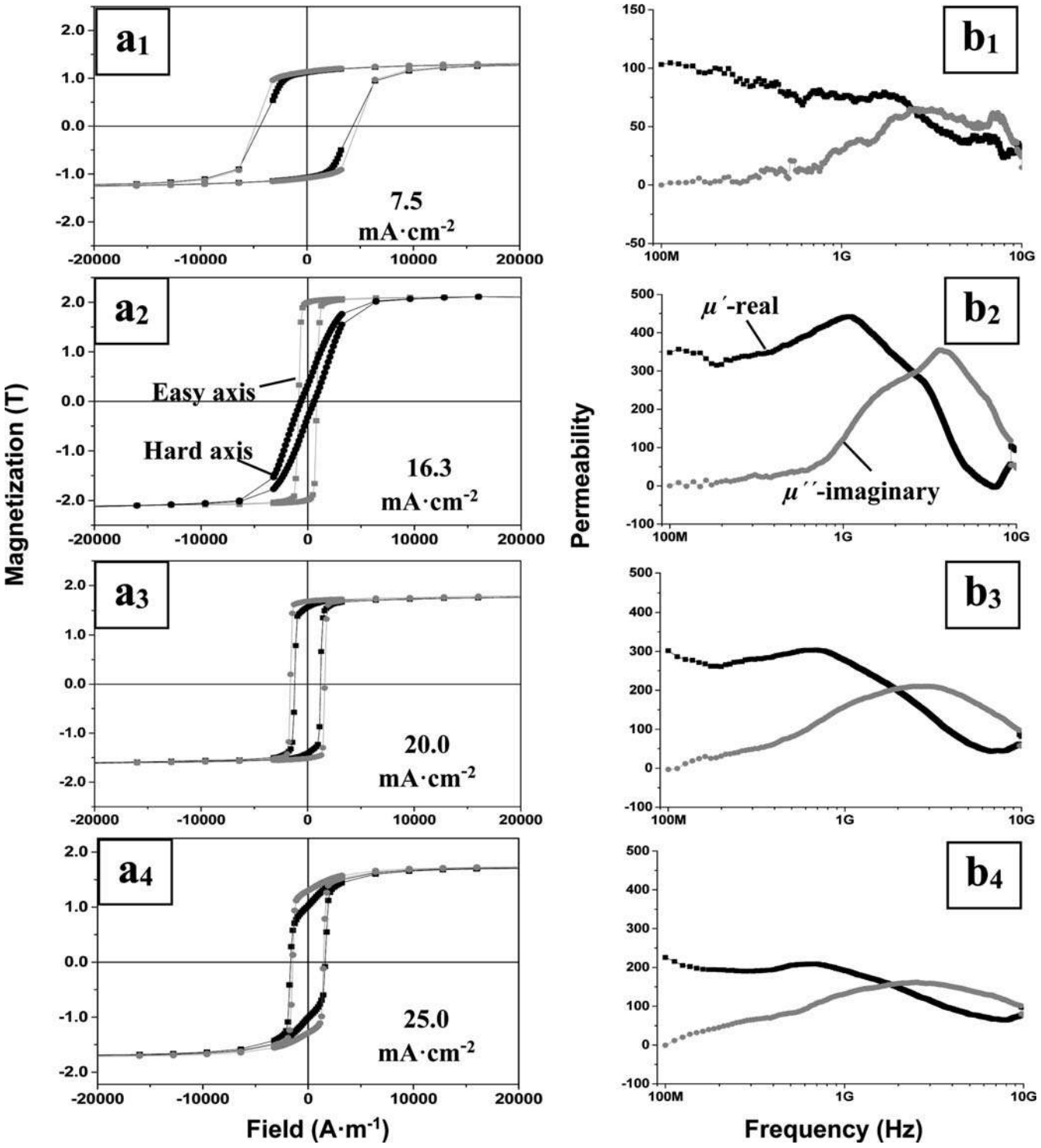

Fig. 3. (a) static *M–H* loops and (b) dynamic μ–f_r curves of the CoFe films electrodeposited at *RT* from a solution containing 1.2 % DMAB and a current density I_d of (1) 7.5, (2) 16.3, (3) 20.0, and (4) 25.0 mA · cm^{-2}, respectively.

concentrations were similar and the individual standard $E^{\circ}_{Co^{2+}/Co}$ (–0.28 V) is higher than $E^{\circ}_{Fe^{2+}/Fe}$ (–0.44 V) in the acidic solution, the atomic Co-ratio was usually larger than Fe-ratio in the anomalously co-deposited CoFe alloys, even from a plating solution containing slightly higher [Fe^{2+}] [33]. This implied that despite the relatively high Fe content (≥ 30 %), the Co content in the as-deposited films was absolutely higher than Fe from the solution with similar [Fe^{2+}] and [Co^{2+}]. This was further confirmed by the EDX measurement results, which indicated a 55 – 70 % Co content in the as-prepared films (Table 1). Due to the high Co content, the films, such as in Fig. $2a_2$–d_2, a_3, c_3, and d_3, possessed a relatively large but moderate anisotropy H_k of 2900 – 8580 A · m^{-1}. Therefore, as predicated theoretically and demonstrated experimentally, the films consisting of fine nanoparticles which were prepared using the relatively high I_d displayed lower H_c, higher saturation magnetization M_s, and moderate anisotropy H_k.

Furthermore, as all the deposited thin CoFe nanofilms possessed in-plane anisotropy, their static and dynamic magnetic properties should be closely related in the unique way according to previous theoretical illustrations. For example, the films in Fig. $2a_2$–d_2, a_3, c_3, inset of b_3, and d_3 with larger M_s, moderate H_k and lower H_c should display desirable microwave properties. The curves in Fig. 3 show the experimental comparison of the static magnetism properties of *M–H* loops and the dynamic microwave properties of μ–f_r curves for the CoFe films, prepared from a series of I_d (shown in Fig. $2c_1$–c_3, and inset of b_3). These curves clearly indicate the detailed responses of the complex permeability (μ'_{max} (real part) and μ''_{max} (imaginary part)) and resonance frequency f_r to the M_s, H_c, and H_k of the CoFe films. For the film fabricated at a low I_d of 7.5 mA · cm^{-2}, which was made up of irregularly shaped particles (Fig. $2c_1$), its large $H_{c\text{-}easy}$ (4400 A · m^{-1}), $H_{c\text{-}hard}$ (4000 A · m^{-1}) and low M_s (1.4 T) (Fig. $3a_1$ and Table 1) corresponded to the poorer dynamic property (Fig. $3b_1$), where the μ'_{max}, μ''_{max}, and f_r are only ∼101, 62, and 2.6 GHz, respectively. With an increase in I_d to 16.3 mA · cm^{-2}, the *M–H* loop in Fig. $3a_2$ demonstrates that the $H_{c\text{-}easy}$ and $H_{c\text{-}hard}$ decrease to the lowest values of 880 and 640 A · m^{-1}, respectively, while the M_s increases to 2.2 T. These changes resulted in the increases in μ'_{max} and μ''_{max} to the largest values of 441 and 355, respectively. The f_r also peaks at 3.9 GHz (Fig. $3b_2$) as the H_k increased to 7360 A · m^{-1}. Thus, these results evidently show that the f_r and μ of the ferromagnetic films were greatly affected by the M_s, H_k, and H_c values, and confirmed the relationships between μ, f_r, M_s, and H_c, as illustrated in Eqs. (1)–(4). When the I_d was further increased to 20.0 mA · cm^{-2}, despite the decline of μ'_{max}, μ''_{max}, and f_r to 303, 210, and 3.1 GHz, respectively (due to the slight increase in H_c and decreases in M_s and H_k), these values were still considerably high. However, with the continuous increase in I_d to 25.0 mA · cm^{-2}, the $H_{c\text{-}easy}$ and $H_{c\text{-}hard}$ slightly changed from 1600 and 1760 A · m^{-1} correspondingly to 1680 and 1360 A · m^{-1}, while the M_s and H_k decreased to 1.6 T and 4800 A · m^{-1}, respectively (Fig. $3a_4$ and Table 1). This change led to a further decline of μ'_{max}, μ''_{max}, f_r and to 225, 162, and 2.5 GHz, respectively (Fig. $3b_4$). Hence the saturation magnetization M_s and anisotropy H_k were the two more critical static magnetism properties affecting the dynamic microwave properties.

Further experiments indicated that the continuous increase in I_d would lead to burnt CoFe films, which surface changed from a shiny silver to dull-gray or black color, with much poorer microwave properties. Therefore, the above experimental results corroborated the theoretical understanding of the relationships between the morphology, deposition parameter, static magnetism and dynamic microwave property of the thin films. For a magnetic soft CoFe film with fine nanoparticles which was prepared from a relatively high (e. g., the middle range of) I_d, the higher M_s and moderate H_k were associated with larger magnetic permeability μ and resonance frequency f_r. The examination results in Table 1 and Fig. 2 from the four plating solutions also revealed that each CoFe film with a unique morphology possessed a distinct magnetic microwave property and the films with similar morphologies exhibited comparable properties. Although the obtained largest M_s, H_k, μ, and f_r values varied with different solutions, the changing trends of the static and dynamic magnetic properties with the morphology were similar.

3.4. Further mechanism analysis and experimental verification

Further mechanism analysis was carried out to elucidate the poorer microwave properties of the CoFe films with the irregular nanoparticles or bigger uniform spherical nanoparticles, produced from both low or high (beyond the middle range of) I_d, respectively. For every pre-assigned plating system or solution, changes in I_d would alter the plating bath potential and over-potentials (increased with I_d) of the ion reductions on the cathode [11, 33], which consequently influenced the behavior and delivery speeds of the metal ions and deposition rate of CoFe crystals. For instance, the measured deposition rate increased from 0.7 (Fig. $2b_1$) to 1.0 nm · s^{-1} (Fig. $2b_2$) when the I_d increasing from 7.5 to 16.3 mA · cm^{-2}. As a result, the change in I_d directly influenced the morphology, crystallinity, particle and grain sizes of the CoFe film. The XRD spectra in Fig. 4 depict the crystallographic structures of the films (Fig. $2c_1$–c_3) prepared from the different plating I_d of 7.5, 16.3, and 20.0 mA · cm^{-2}, respectively. As the XRD peak intensities have been normalized based on the CoFe film thickness, the peak density indicated the extent of crystallization (viz., crystallinity) for each film. All the films prepared from the solution containing 1.2 % DMAB at room temperature consisted almost entirely of CoFe (110) crystals. However, residual traces of Fe_2O_3 (214) crystals were also observed. From the downward trend of the ratio of the sharp to the broad peak intensity at different I_d, it appears that the crystallinity for the CoFe film at higher I_d was poorer than that at lower I_d. From the viewpoint of electrochemical deposition, the decrease in crystallinity is due to the greater extent of vacancies or other crystal defects at higher depositing rate [11, 35], which arose from the higher I_d. A reduction in crystallinity would result in lower anisotropy.

To compare the changes of grain and particle sizes with the increase in I_d, the mean grain sizes (τ) for this series of films fabricated at different I_d were calculated using the Scherrer equation. [37], which is shown as follows:

$$\tau = k\lambda/(\beta \cos\theta) \quad (5)$$

where λ is X-ray wavelength (0.15406 nm), k is a constant related to grain shape (typical value 0.9), θ is the Bragg angle (half of 2θ, which corresponds to the tip of the peak), and β is the peak width at the half maximum height. The values of θ and β for the $Fe_{33}Co_{67}$, $Fe_{43}Co_{57}$, and $Fe_{45}Co_{55}$ films (Fig. 4a–c) are summarized in Table 2, along with the corresponding calculated grain sizes (τ) of 22.9, 21.5, and 22.1 nm, respectively. Though the plating I_d varied for the films, the calculated grain sizes remained similar. This shows that the films with relatively uniform fine nanoparticles (e. g., in Fig. $2a_2$–d_2, a_3–d_3 and inset of b_3) contained fine homogeneous grains, hence possessing the lower H_c [13, 23]. In addition, for varying I_d, the trend in the grain size was unlike that of the particle size observed in the CoFe films. This implied that with the increase in particle size (or the increase in I_d) and the decrease of crystallinity, a greater extent of amorphous CoFe components wrapped or combined with the CoFe grain domains in the films. This led to the decrease in crystalline anisotropy (H_k) and the saturated magnetization (M_s), as more vacancies or other crystal defects were present and the extent of compact piling of CoFe atoms was weaker in the amorphous phase. As such, a much higher current density I_d resulted in relatively lower M_s and H_k. This explains the fact that although the films produced at the high I_d consisted of uniform spherical particles with low H_c (e. g., down to 880 A · m^{-1}) (Table 1), they displayed poorer microwave properties than those produced at the middle range of I_d. In the case of films fabricated at low I_d, even though a higher crystallinity (Fig. 4a) was obtained, the resultant lower Fe atom-ratio led to lower M_s. In addition, the irregular CoFe particles also led to the inhomogeneous size grains and poorer exchange coupling [13, 29], and subsequently higher H_c as well as the nearly negligible magnetic anisotropy between easy and hard axes. These factors caused the deterioration of the microwave properties of the films. The results were further verified by the theoretically estimated ferromagnetic resonance (f_{rEsti}) in hard axis from Eq. (3) for these in-plane anisotropic ferromagnetic thin films, as listed in Table 1. The calculated values for f_{rEsti} are obviously higher than the measured ones. This should be caused by the damping effect, which is neglected in Eq. (1) and (3) [25]. As a larger damping effect resulted from more inhomogeneity of the thin films, which was caused by the crystal–amorphous phase mixture, foreign oxides, and different particle or grain sizes, the difference between measured f_r and f_{rEsti} for the films from the low and high I_d was usually larger than that for the films from the middle I_d in all series solutions. Therefore, because of the drawbacks of both high and low I_d, only the CoFe films, made up of uniform fine spherical particles with higher crystallinity which were produced from the middle range of I_d, possessed the lowest H_c, moderate H_k and largest M_s, as well as the best microwave properties.

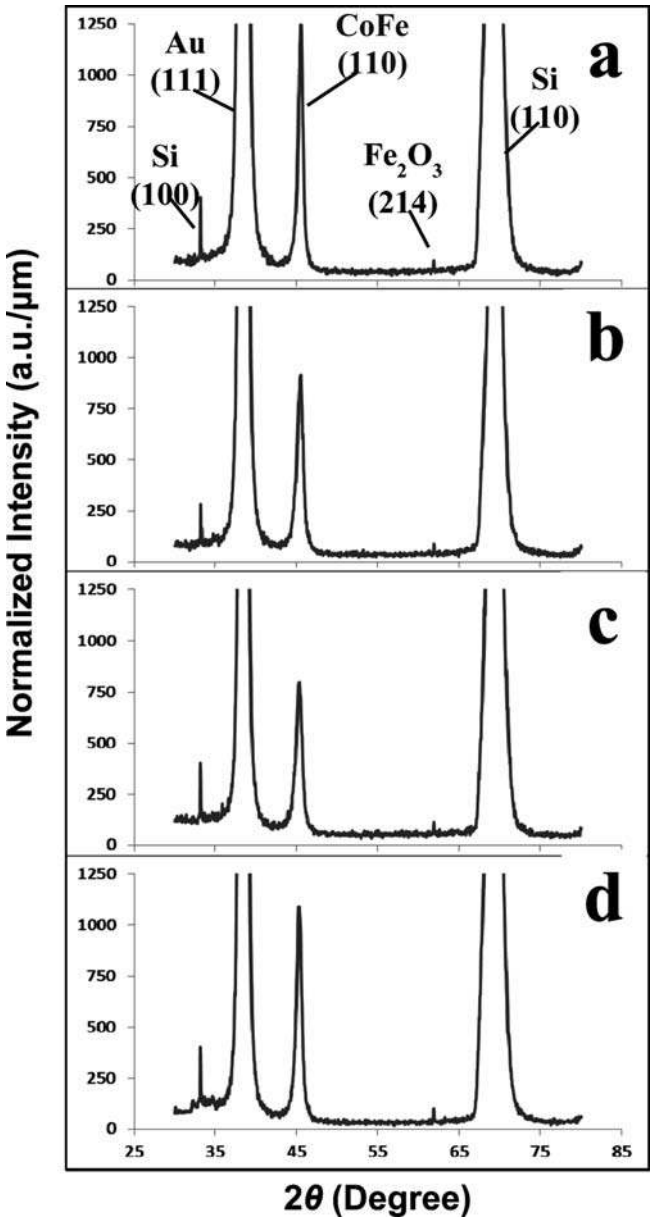

Fig. 4. 2θ XRD results of (a) $Fe_{33}Co_{67}$, (b) $Fe_{43}Co_{57}$, and (c) $Fe_{45}Co_{55}$ films on 30 nm Au(111)/5 nm Ta/Si substrates. The films were electrodeposited from the solution containing 1.2 % DMAB additive at *RT* and an I_d of (a) 7.5, (b) 16.3, and (c) 20.0 mA · cm^{-2}, respectively. (d) Annealed $Fe_{45}Co_{55}$ film at 250 °C for 1 h under in-plane easy-axis magnetic field of 1 T.

Previous studies indicated that suitable annealing treatments can improve the particle uniformity and crystallinity of the thin deposited films [15, 38]. The FESEM images of Fig. 5a–d illustrate morphologies of the CoFe films, which previous corresponding images are Fig. $2a_3$–d_3, after vacuum annealing at 250 °C for 1 hour under an in-plane magnetic field of 1 T (Fig. 1). More uniform nanoparticle morphologies and increased crystallinity (Fig. 4d) were ob-

Table 2. The measured parameters and calculated mean grain sizes according to the Scherrer equation from the XRD peaks of three CoFe films.

Film	Bragg angle θ	Peak width β	Grain size, τ (nm)
$Fe_{33}Co_{67}$	22.7°	0.75° (or 0.00654)	22.9
$Fe_{43}Co_{57}$	22.7°	0.80° (or 0.00698)	21.5
$Fe_{45}Co_{55}$	22.6°	0.78° (or 0.00681)	22.1

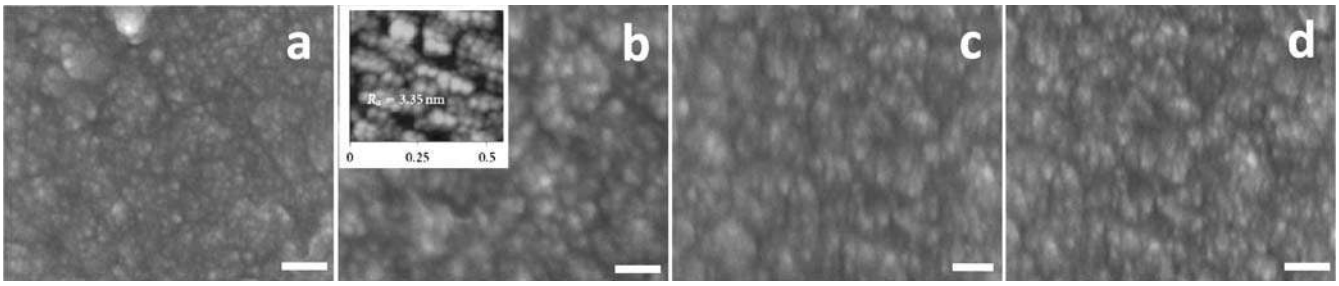

Fig. 5. FESEM images of four thin CoFe films (a–d), which were annealed at 250 °C for 1 h in vacuum under an in-plane magnetic field of 1 T along the easy axis direction. The films were previousely electrodeposited from the four series of plating solutions and a current density I_d of 25.0, 25.0, 20.0, and 20.0 mA · cm^{-2}, respectively. The scale bars are 100 nm. The inset image of (b) is the corresponding 0.6 × 0.6 μm AFM image.

Table 3. The magnetism, microwave, and other properties of the annealed CoFe films fabricated from the solution containing 1.2 % DMAB at *RT*.

Plating solution	I_d (mA · cm^{-2})	M_s (T)	H_k (A · m^{-1})	μ'_{max}	μ''_{max}	f_r (GHz)	Surface	ρ (× 10^{-5}, Ω · cm)
1.2 % DMAB, *RT*	7.5	1.5	7 600	218	179	3.0	Shining & no micro-crack	3.5
	16.3	2.3	8 000	509	365	2.2		5.0
	20.0	1.9	7 680	592	389	1.0		4.9
	25.0	1.7	7 200	318	224	3.9		4.8

Note: Annealing was conducted at 250 °C in a vacuum oven for 1 hour.

served after the annealing process. As such, an improvement of microwave properties for the films can be expected after annealing based on the above analyses. For instance, the data in Table 3 show the significantly improved dynamic microwave properties for the "c" series of CoFe films (Fig. 2c) at all I_d after annealing. For the films prepared from the middle range I_d, all the complex permeability μ increased significantly. In the case of the films prepared at the low and high I_d, both the μ and resonance frequency f_r were increased. A largest μ'_{max} value of 592 was also obtained from the aggregated fine nanoparticle film. In particular, for the film prepared at the high I_d of 25.0 mA · cm^{-2}, the μ'_{max}, μ''_{max}, and f_r increased significantly from pre-annealed values of 225, 162, and 2.3 GHz to correspondingly post-annealed values of 318, 224, and 3.9 GHz, due to the increased crystallinity, M_s and H_k after the annealing. As shown in Table 3, these annealed films also possess other desirable physical and electrical properties, such as shiny surfaces without micro-cracks and relatively high resistivity ρ. Therefore, the preparation of spherical granular films using suitable deposition parameters and annealing process produced the desirable properties for different microwave applications in the high frequency of GHz range.

4. Conclusions

In summary, based on theoretical analyses, CoFe films, consisting of uniform fine spherical nanoparticles and large magnetic permeability (real part up to ∼600) as well as resonance frequency (up to ∼5 GHz) have been rapidly prepared. The films could be obtained from different simple sulfate/chloride-based solutions at similar Fe^{2+} and Co^{2+} concentrations by tuning the plating current density at the higher middle range. Annealing under a magnetic field with easy-axis direction could further enhance the microwave properties of the thin films through improving the crystallinity. From the experimentally revealed relationships between the surface morphology, deposition parameters, and static magnetism as well as dynamic microwave properties, identifying the microwave properties of thin CoFe films from their nanomorphologies and electrodeposition parameters became possible. These methodologies are practical in the quick development and fabrication of thin CoFe or other soft ferromagnetic films for gigahertz microwave applications.

The authors thank Dr C. R. Deng and Mr S. K. Ting for the kind help and instructions.

References

[1] N. Setter: Electroceramic-based MEMS. Springer Science+Business Media, Inc, USA (2005). DOI:10.1007/b101200
[2] N. Maluf, K. Williams: An Introduction to microelectromechanical systems engineering, 2nd Edn., Artech House, U.K. (2004).
[3] D. Hunter, W. Osborn, K. Wang, N. Kazantseva, J. Hattrick-Simpers, R. Suchoski, R. Takahashi, M.L. Young, A. Mehta, L.A. Bendersky, S.E. Lofland, M. Wuttig, I. Takeuchi: Nature Commun. 2 (2011) 518. DOI:10.1038/ncomms1529.
[4] M. Frommberger, A. Ludwig, A. Sehrbrock, E. Quandt: IEEE Trans. Magn. 39 (2003) 3166. DOI:10.1109/TMAG.2003.816045
[5] M.A.S.M. Haniff, H.W. Lee, D.C.S. Bien, I.H.A. Azid, M.W. Le, S.S. Embong: Thin Solid Films 550 (2014) 22. DOI:10.1016/j.tsf.2013.10.020
[6] A. Kumar, P.C. Srivastava: J. Exp. Nanosci. 10 (2015) 803. DOI:10.1080/17458080.2014.902543.
[7] W. Lu, P. Huang, C.H. He, B. Yan: Int. J. Electrochem. Sci. 8 (2013) 914.

[8] J. Zarpellon, H.F. Jurca, N. Mattoso, J.J. Klein, W.H. Schreiner, J.D. Ardisson, W.A.A. Macedo, D.H. Mosca: J. Colloid Interf. Sci. 316 (2007) 510. DOI:10.1016/j.jcis.2007.08.032
[9] W.N. Yu, J.A. Bain, Y.G. Peng, D.E. Laughlin: IEEE Trans. Magn. 38 (2002) 3030. DOI:10.1109/TMAG.2002.802126
[10] L. Guo, G. Oskam, A. Radisic, P.M. Hoffmann, P.C. Searson: J. Phys. D: Appl. Phys. 44 (2011) 443001. DOI:10.1088/0022-3727/44/44/443001.
[11] M. Schlesinger, M. Paunovic: Modern electroplating. 5th Ed., John Wiley & Sons Ltd, Weinheim, Germany (2010). DOI:10.1002/9780470602638
[12] A. Mardana, S. Ducharme, S. Adenwalla: Nano Lett. 11 (2011) 3862. DOI:10.1021/nl201965r
[13] G. Herzer: IEEE Trans. Magn. 26 (1990) 1397. DOI:10.1109/20.104389
[14] F.M.F. Rhen, S. Roy: IEEE Trans. Magn. 44 (2008) 3917. DOI:10.1109/TMAG.2008.2002254
[15] B.Y. Zong, Z.W. Pong, Y.P. Wu, P. Ho, J.J. Qiu, L.B. Kong, L. Wang, G.C. Han: J. Mater. Chem. 21 (2011) 16042. DOI:10.1039/c1jm13398e
[16] Z. Turgut, J.H. Scott, M.Q. Huang, S.A. Majetich, M.E. McHenry: J. Appl. Phys. 83 (1998) 6468. DOI:10.1063/1.367922
[17] S.H. Jung, J.W. Yeon, K. Song: J. Solid State Electrochem. 18 (2014) 333. DOI:10.1007/s10008-013-2357-z
[18] Z. He, J.A. Koza, G.J. Mu, A.S. Miller, E.W. Bohannan, J.A. Switzer: Chem. Mater. 25 (2013) 223. DOI:10.1021/cm302823f
[19] G.Z. Chai, D.W. Guo, X.L. Fan, D.S. Xue: Sci. China Phys. Mech. Astron. 54 (2011) 1200. DOI:10.1007/s11433-011-4356-3
[20] N. Zech, E.J. Podlaha, D. Landolt: J. Appl. Electrochem. 28 (1998) 1251. DOI:10.1023/A:1003416328942
[21] J.K. Dong, Y. Tokiwa, S.L. Bud'ko, P.C. Canfield, P. Gegenwart: Phys. Rev. Lett. 110 (2013) 176402. DOI:10.1103/PhysRevLett.110.176402
[22] F.M.F. Rhen, P. McCloskey, T. O'Donnell, S. Roy: J. Magn. Magn. Mater. 320 (2008) 819. DOI:10.1016/j.jmmm.2008.04.133
[23] B.Y. Zong, G.C. Han, J.J. Qiu, Z.B. Guo, L. Wang, W.K. Yeo, B. Liu: Res. Lett. Phys. Chem. 2008 (2008) Article ID 342976. DOI:10.1155/2008/342976.
[24] O. Acher, S. Dubourg: A generalization of Snoek's law to ferromagnetic films and composites, CEA Le Ripault, BP16 : 37260 Monts, France (2007) 1 – 22.
[25] Y. Liu, D.J. Sellmyer, D. Shindo: Handbook of advanced magnetic materials, Spin 11097730, Springer Verlag, New York (2006) 418 – 455. DOI:10.1007/b115335
[26] S.X. Wang, N.X. Sun, M. Yamaguchi, S. Yabukami: Nature 407 (2000) 150. DOI:10.1038/35025140
[27] P.S. Fodor, G.M. Tsoi, L.E. Wenger: J. Appl. Phys. 91 (2002) 8186. DOI:10.1063/1.1449450
[28] E.F. Kneller, F.E. Luborsky: J. Appl. Phys. 34 (1963) 656. DOI:10.1063/1.1729324
[29] S.R. Brankovic, X.M. Yang, T.J. Klemmer, M. Seigler: IEEE Trans. Magn. 42 (2006) 132. DOI:10.1109/TMAG.2005.861778
[30] Y.H. Zhang, D.G. Ivey: Chem. Mater. 16 (2004) 1189. DOI:10.1021/cm0305507
[31] N. Zech, E.J. Podlaha, D. Landolt: J. Electrochem. Soc. 146 (1999) 2892. DOI:10.1149/1.1392024
[32] N. Zech, E.J. Podlaha, D. Landolt: J. Electrochem. Soc. 146 (1999) 2886. DOI:10.1149/1.1392024
[33] S.R. Brankovic, S.E. Bae, D. Litvinov: Electrochim. Acta 53 (2008) 5934. DOI:10.1016/j.electacta.2008.03.071
[34] W. Schwarzacher: J. Phys. Condens. Matter. 16 (2004) R859. DOI:10.1088/0953-8984/16/26/R01
[35] M. Lelental: J. Electrochem. Soc. 120 (1973) 1650. DOI:10.1149/1.2403322
[36] U. Holzwarth, N. Gibson: Nature Nanotech. 6 (2011) 534. DOI:10.1038/nnano.2011.145
[37] T. Bitoh, A. Makino, A. Inoue, T. Masumoto: Mater. Trans. 44 (2003) 2011. DOI:10.2320/matertrans.44.2011
[38] S.M. Abbasi, A. Momeni, M. Morakkabati, R. Mahdavi: Int. J. Mater. Res. 105 (2014) 755. DOI:10.3139/146.111078

(Received March 6, 2015; accepted April 20, 2015)

Correspondence address

Dr BaoYu Zong
Temasek Laboratories
National University of Singapore
#09-02, T Lab Building
5A Engineering Drive 1
Singapore 117411
Tel.: +65 66011072
Fax: +65 6872 6840
E-mail: tslzb@nus.edu.sg

Bibliography
DOI 10.3139/146.111273
Int. J. Mater. Res. (formerly Z. Metallkd.)
106 (2015) E; page 1 – 9

ISSN 1862-5282